Tree Physiology 32, 1161–1170
doi:10.1093/treephys/tps071

Research paper

Hydraulic efficiency and safety of vascular and non-vascular components in *Pinus pinaster* leaves

Katline Charra-Vaskou[1,6], Eric Badel[2,3], Régis Burlett[4,5], Hervé Cochard[2,3], Sylvain Delzon[4,5] and Stefan Mayr[1]

[1]Department of Botany, University of Innsbruck, Sternwartestr. 15, A-6020 Innsbruck, Austria; [2]INRA, UMR A547 PIAF, Site INRA de Crouelle, 5 chemin de Beaulieu, F-63100 Clermont-Ferrand, France; [3]Clermont Université, Université Blaise Pascal, UMR A547 PIAF, F-63000 Clermont-Ferrand Cedex 2, France; [4]INRA, UMR 1202 BIOGECO, F-33610 Cestas, France; [5]Université de Bordeaux, UMR 1202 BIOGECO, F-33610 Cestas, France; [6]Corresponding author (katline.charra-vaskou@uibk.ac.at)

Received January 11, 2012; accepted July 9, 2012; published online August 19, 2012; handling Editor Roberto Tognetti

Leaves, the distal section of the soil–plant–atmosphere continuum, exhibit the lowest water potentials in a plant. In contrast to angiosperm leaves, knowledge of the hydraulic architecture of conifer needles is scant. We investigated the hydraulic efficiency and safety of *Pinus pinaster* needles, comparing different techniques. The xylem hydraulic conductivity (k_s) and embolism vulnerability (P_{50}) of both needle and stem were measured using the cavitron technique. The conductance and vulnerability of whole needles were measured via rehydration kinetics, and Cryo-SEM and 3D X-ray microtomographic observations were used as reference tools to validate physical measurements. The needle xylem of *P. pinaster* had lower hydraulic efficiency ($k_s = 2.0 \times 10^{-4}$ m^2 MPa^{-1} s^{-1}) and safety ($P_{50} = -1.5$ MPa) than stem xylem ($k_s = 7.7 \times 10^{-4}$ m^2 MPa^{-1} s^{-1}; $P_{50} = -3.6$ to -3.2 MPa). P_{50} of whole needles (both extra-vascular and vascular pathways) was -0.5 MPa, suggesting that non-vascular tissues were more vulnerable than the xylem. During dehydration to -3.5 MPa, collapse and embolism in xylem tracheids, and gap formation in surrounding tissues were observed. However, a discrepancy in hydraulic and acoustic results appeared compared with visualizations, arguing for greater caution with these techniques when applied to needles. Our results indicate that the most distal parts of the water transport pathway are limiting for hydraulics of *P. pinaster*. Needle tissues exhibit a low hydraulic efficiency and low hydraulic safety, but may also act to buffer short-term water deficits, thus preventing xylem embolism.

Keywords: cavitation, collapse, conductivity, conifer, extra-vascular pathway, microtomography, needle, vulnerability, xylem, 3D visualization.

Introduction

Water transport in trees follows the water potential gradient between the soil and the atmosphere, according to the cohesion–tension theory (Tyree and Zimmermann 2002). The sections of the transport pathway are known to differ in their hydraulic safety and efficiency. Leaves, as the distal part of the soil–plant–atmosphere continuum, play a key role in plant hydraulics.

Xylem sap is transported under negative pressure, so that plants risk embolism (Cochard and Tyree 1990, Sperry and Tyree 1990, Tyree et al. 1994) or collapse of conduits (Hacke et al. 2001, Cochard et al. 2004*a*, see also Brodribb and Holbrook 2005). Both types of dysfunction affect hydraulic efficiency, i.e., specific hydraulic conductivity (Tyree and Zimmermann 2002). Sufficient hydraulic conductivity is especially important in trees to maintain moderate decreases in water potential along the extended transport pathways. Drought-induced embolism occurs when the water potential (P) in tracheids falls below xylem-specific thresholds, at which point air enters from adjacent, already air-filled spaces ('air seeding'; Tyree and Zimmermann 2002). These thresholds are determined

by the structure of pit membranes, because air seeding occurs via the pits (Sperry and Tyree 1988, Cochard et al. 2009, Delzon et al. 2010). It has been shown for several species that vulnerability to drought-induced embolism varies within trees (Tyree and Sperry 1988, Tyree and Zimmermann 2002, Mayr et al. 2003). This vulnerability pattern allows trees to optimize their hydraulic architecture, enabling them for example to sacrifice branches under drought conditions (Tyree and Zimmermann 2002). Xylem collapse, observed so far only in leaves, occurs when transversal mechanical wall support is not strong enough to withstand negative hydrostatic pressure exerted on walls (Hacke et al. 2001, Cochard et al. 2004*a*, Brodribb and Holbrook 2005). Mechanical reinforcement in stems probably also prevents conduit deformation under low water potentials before the rupture of water columns. Collapse and cavitation events both lead to a decrease in hydraulic conductivity, but up to now only few studies on vulnerability to drought-induced embolism distinguish between the two (Hukin et al. 2005, Woodruff et al. 2007, Brodribb and Cochard 2009, Johnson et al. 2012).

Numerous studies have meanwhile dealt with the hydraulic efficiency and safety of angiosperm leaves (i.e., Salleo et al. 2000, Choat et al. 2005, Hao et al. 2008, Chen et al. 2009). According to Sack and Holbrook (2006), 30–80% of whole plant hydraulic resistance is located in leaves (Tyree et al. 1981, Yang and Tyree 1994, Sack et al. 2003) and Nardini and Salleo (2000) reported 92% of the total resistance of *Laurus nobilis* L. shoots to be in the leaves. Under drought conditions, conductivity of leaves decreases, as in stems, but the vulnerability of leaves is higher than that of stems (Woodruff et al. 2007, Chen et al. 2009). Brodribb and Holbrook (2004) reported a mid-day depression of leaf conductance (K_{leaf}) between 40 and 50% of pre-dawn values on days of high evaporative demand, and Hao et al. (2008) found a higher vulnerability in leaves than in stems in six species. Sack et al. (2004, 2005) demonstrated that 11–74% of whole leaf resistance was located in the leaf xylem. Other authors (e.g., Trifilo et al. 2003, Cochard et al. 2004*b*, Gasco et al. 2004, Nardini et al. 2005) found the leaf xylem resistance to be of minor importance compared with the extra-vascular pathway (see also Brodribb et al. 2007, Blackman and Brodribb 2011).

In contrast to angiosperms, knowledge of conifer needles is still scant. It was shown for *Picea abies* (L.) Karst that stem and needle xylem exhibited similar specific conductivities and for *Pinus mugo* that 24% of the total needle resistance was located in the xylem (Charra-Vaskou and Mayr 2011). There are also only a few studies on needle vulnerability: based on Cryo-SEM observations, Cochard et al. (2004*a*) observed, in needles of four different species, a progressive collapse of tracheids during dehydration below a specific threshold pressure, which correlated with the onset of cavitation in the stems. Loss of conductance occurred at very high leaf water potential in *Pinus taeda* L. needles (P_{50} around –1 MPa; Domec et al. 2009), and Johnson et al. (2009) analysed embolism formation in *Pinus ponderosa* C. Lawson and *Pinus nigra* Arnold needles (P_{50}–1.65 and –1.52 MPa, respectively). Up to now, information on vulnerability patterns within needles has been completely lacking.

In this study, we analysed the hydraulic safety and efficiency of *Pinus pinaster* Ait. needles with the cavitron technique, a method commonly used to measure vulnerability to drought-induced embolism of stems, and with ultrasonic acoustic emission analysis. Based on a comparison with the rehydration method, we also estimated the hydraulic properties of the vascular and extra-vascular components within the needle. Cryo-SEM analysis and X-ray observation, which supplied three-dimensional pictures, allowed analysis of needle tissue structures under drought stress.

We hypothesized a higher vulnerability to drought in needles than in stem xylem with needle collapse occurring before embolism formation in the needle xylem (Cochard et al. 2004*a*). The extra-vascular pathway within the needle was expected to represent a major part of total needle resistance and to be also affected by drought stress, e.g., by a collapse of parenchyma cells.

Materials and methods

Materials

Sun twigs of *P. pinaster* were harvested in September and October 2010 at the campus of the University of Bordeaux, Talence (France) between 8:00 and 10:00 a.m., immediately wrapped in plastic bags and transferred to the laboratory. Branches were re-cut under water and rehydrated for 24 h. One-year-old needles were used for measurements to avoid any impairment of conductivity due to needle age (Charra-Vaskou and Mayr 2011) (*P. pinaster* needle life span is 3–5 years).

Centrifuge measurements

In stems and needles, vulnerability of drought-induced embolism was determined using the cavitron technique as described in Cochard et al. (2005) and Beikircher et al. (2010). This technique is based on centrifugal force, which increases water tension in a xylem segment, while loss of conductance is simultaneously measured. All measurements were made at the high-throughput phenotyping platform of the University of Bordeaux, Talence, France (http://sylvain-delzon.com/caviplace).

For stem measurements, segments were fixed in a custom-built rotor of diameter 0.30 m (Honeycomb, Precis 2000, University of Bordeaux, Talence, France) mounted on a high-speed centrifuge (Sorvall RC5 plus, MSE Scientific, London, UK). The sample ends were positioned in upstream and downstream reservoirs filled with distilled degassed water containing

$CaCl_2$ (1 mM) and KCl (10 mM). The centrifugation speed was increased in 0.5 MPa steps to expose samples to increasing tensions. Conductance (k) was measured three times at each step. The procedure was repeated for at least eight pressure steps until loss of conductance reached at least 90%. Vulnerability curves (VCs) were obtained from percentage loss of conductance (PLC) versus xylem pressure (P) plots, with PLC computed as

$$PLC = 100(1 - k/k_{max}) \quad (1)$$

with k and k_{max} corresponding to the actual and maximum hydraulic conductance, respectively. The rotor velocity was monitored with a 10 rpm resolution electronic tachymeter (A2108-LSR232, Compact Inst, Bolton, UK), and xylem pressure was adjusted to ~± 0.02 MPa. We used the Cavi_soft software (version 2.1, University of Bordeaux, Talence, France) for data acquisition and conductance computation.

Vulnerability curves were obtained by plotting fractional (%) loss of conductance versus xylem pressure. Curves were fitted using an exponential sigmoidal equation given in Pammenter and Vander Willigen (1998):

$$y = \frac{100}{\left[1 + \exp\left(S/25 \times \left(P - P_{50}\right)\right)\right]} \quad (2)$$

where y is the PLC, P is the corresponding xylem pressure (MPa) and S is related to the slope of the curve. P_{50} is the P value corresponding to 50% loss of conductance. Vulnerability curves were calculated using the software Fig. P. 2.98 (Biosoft Corp., Cambridge, UK).

For needle measurements, stem samples 16–18 cm long were left for at least 1 h in cold water (5 °C) to avoid interference of resin with the sap conductivity measurement, and re-cut two or three times at 15 min intervals. Twenty needles of 14.5 cm (after cutting) were inserted in reservoirs, and the cavitron was cooled to 5 °C and maintained at this temperature during measurements (Cochard et al. 2000*b*). Although Cochard et al. (2007) reported that temperature effects on xylem vulnerability were negligible on *Taxus baccata* L. (e.g., regarding surface tension, changes in pit membrane porosity or in microfibril rigidity in pit margo), some impact of the temperature on needle measurements could be totally ruled out. Unfortunately, it was not possible to overcome the resin problems with another methodical setup. Cavitron measurements proceeded with a 0.15 m diameter custom-built rotor (Precis 2000, University of Bordeaux) as described above.

Xylem hydraulic conductivities (k_s, $m^2\ s^{-1}\ MPa^{-1}$) for both stems and needles were computed from cavitron flow measurements (corresponding to k_{max}) related to sample length and xylem cross-sectional area. Temperature correction for water density was made according to Cochard et al. (2000*b*). The xylem area in needles was determined from microscopic pictures of cross sections (ImageJ 1.37, public domain, National Institutes of Health, Bethesda, MD, USA).

Analysis of ultrasonic emission

Saturated branches were dehydrated on the bench, while ultrasonic emissions (UEs) (Johnson et al. 2009, Mayr and Rosner 2011) from the main stem and needles were recorded and, at intervals, P value of needles was determined.

Ultrasonic sensors (150 kHz resonance sensors, R15/C, 80–400 kHz) were attached on the main stem and on needles of saturated branches. On the upper side (opposite wood) of the main stem, 3 cm^2 of the bark was removed (~10 cm from the base) and the xylem was covered with silicone grease (to improve acoustic coupling and prevent transpiration). R15C sensors were then attached with clamps (plastic-coated metal springs). For measurements on needles, three neighbouring needles of an end twig were positioned in parallel on a glass plate and covered with silicone grease. A R15C sensor was placed on the needles and loaded with an 88 g weight to block it. Sensors were connected to a 20/40/60 dB preamplifier set to 40 dB and to an 8-channel PCI-2 system (PAC 125 18-bit A/D, 3 kHz to 3 MHz PCI2; all components of the UE system from Physical Acoustics Corporation, Wolfegg, Germany). Detection threshold was set at 45 dB for needles and stems, and the peak definition time, hit definition and hit lockout time were 200, 400 and 2 µs, respectively. Recording and analysis of UEs used AEwin software (Physical Acoustics Corporation, Wolfegg, Germany). We note that the effective contact area between the sensor and sample could not be controlled, so that the coupling pressure, which influences the intensity of registered signals, could be neither adjusted nor determined (see also Mayr and Sperry 2010).

Four ultrasonic sensors were placed on the needles and one on the stem of each dehydrating twig, respectively. P was measured at intervals with a pressure chamber (Model 1000 Pressure Chamber; PMS Instrument Company, Corvallis, OR, USA) on needles carefully cut from dehydrating branches so that no artificial UEs were caused. Measured values were assumed to be similar to P in the whole branch, as transpiration was low.

For vulnerability analysis, the cumulative number of UEs corresponding to the measured P value was related to the total number of UEs until all acoustic activity ceased. Vulnerability curves were obtained by plotting the cumulative number of UEs (%) versus the xylem pressure (P) and were fitted using the exponential sigmoidal equation (2), where y is the cumulative UE number, P is the corresponding xylem pressure and parameter S is related to the curve slope. P_{50} corresponds to P at 50% of the maximum cumulative UE value. The VCs were calculated using Fig. P 2.98 (Biosoft Corp.).

Rehydration kinetics analysis

The experimental procedure followed Brodribb and Holbrook (2003). First, the capacitance (C; mol m^{-2} MPa^{-1}) of needles was quantified by dehydration of single needles and repeated measurements of weight (Sartorius ME2355, precision 0.01 mg, Sartorius AG, Germany) and corresponding P, which was determined with a pressure chamber (Model 1000 Pressure Chamber, PMS Instrument Company). Needle weight at saturation and needle dry weight were used for the calculation of relative water content (RWC, dimensionless, 1 at saturation). Second, for conductivity measurements at different dehydration steps, shoots were enclosed in plastic bags for at least 1 h to equilibrate P within needles before P was determined on cut needles with the Scholander technique (P_0). One needle was then cut under water from each shoot for the rehydration procedure: The needle bases (ca. 2 mm) were placed in a tray with distilled water, the needles were left to recharge for 5–500 s and P was measured (P_t). The needle conductance K_{leaf} (mol m^{-2} s^{-1} MPa^{-1}) was calculated from Eq. (3):

$$K_{leaf} = C \times \ln(P_0/P_t) \times t^{-1} \quad (3)$$

where C is the capacitance (mol m^{-2} MPa^{-1}), P_0 and P_t are the P values (Pa) before and after rehydration for the time span t (s). The capacitance is species-specific and was 1.312 mol m^2 MPa^{-1} for *P. pinaster* between 0 and –1.5 MPa.

Test measurements were made to exclude negative effects due to resin, as lower conductivity by xylem obstruction or higher conductivity by water passing through resin channels might occur (data not shown): No effect on flow measurements was observed, either when needles were repeatedly trimmed during rehydration to remove possible resin blockage, or when rehydration kinetics were followed at a temperature of 5 °C (to avoid emptying of channels). The procedure used for rehydration measurements was thus expected to enable accurate determination of K_{leaf}.

Vulnerability curves were obtained by plotting fractional (%) loss of conductance versus xylem pressure. Curves were fitted using an exponential sigmoidal equation (Eq. (2)), where y is the PLC, P is the corresponding xylem pressure (Pa) and S is related to the slope of the curve. P_{50} is the P value corresponding to 50% loss of conductivity. Percentage loss of conductance was calculated from the ratio of actual (at a given P) to maximum (i.e., first measurement at –0.41 MPa) K_{leaf}. Vulnerability curves were calculated using Fig. P 2.98 (Biosoft Corp.).

Cryo-SEM

Xylem structures were analysed on fully hydrated needles and needles dehydrated to –2 or –4 MPa. Needles were detached from dehydrated shoots and immediately soaked in a bath of liquid N_2. Segments ~2 cm long were taken from the central part of each needle and stored at –80 °C until observation. The samples were thus frozen while the xylem pressure in the needles was close to that before excision.

Observations were made with an SEM (model SEM 505, Philips, Eindhoven, The Netherlands) equipped with a cryogenic stage (model CT 1000, Hexland, Oxford Instruments Ltd, Oxford, UK) at the Electron Microscopy Laboratory of the Institut National de la Recherche Agronomique, Theix (Clermont-Ferrand, France). This equipment enables observations of xylem content on intact frozen samples (Cochard et al. 2000*a*, Mayr and Cochard 2003, Johnson et al. 2009). Samples stored at –80 °C were first immersed in liquid N_2 and placed in holes 1 cm deep in a sample holder. The samples were then rapidly transferred to a cryo chamber for a step at –180 °C. Once vacuum was reached in the chamber, the samples were cryofractured inside the chamber to expose the vascular bundles on the cross sections. This procedure considerably reduced the deposition of frost on the cross sections. The samples were then transferred to the SEM chamber and installed for a cooling step at –160 °C. Samples were first observed at a low voltage (<5 kV), and the presence of ice or air in the tracheids was noted. To delineate cell walls more precisely, the samples were then etched by raising the SEM step temperature to –80 °C. Finally, the samples were coated with a gold deposit in the cryo chamber (–180 °C). Coating was necessary to obtain high-resolution and contrasted pictures, but it often had the effect of subliming away most of the ice in the tracheids. However, we checked that ice sublimation had no effect on wall shape, the samples always remaining below –80 °C.

3D X-ray microtomography

Three-dimensional pictures of needles were acquired with an X-ray nanotomograph (Nanotom 180 XS, GE, Wunstorf, Germany) at the PIAF laboratory of the Institut National de la Recherche Agronomique, Theix (Clermont-Ferrand, France). This non-destructive method is based on the local X-ray absorption behaviour of the sample mainly according to its density, and allows the observation of the internal structure without surface or thin slice preparation.

Branches were dehydrated on the bench and a pair of needles was cut from the branches at intervals. Xylem pressure was determined on one needle with a pressure chamber (PMS Instrument Company) and pictures were obtained with the second needle. The needle was first wrapped in a paraffin film to prevent drying during image acquisition. The field of view was ~2.5 × 2.5 × 2.5 mm^3 in the centre of the 20 cm needle and covered its full cross section. X-ray parameters were 60 kV and 240 µA. We used a molybdenum target to increase the contrast for low-density tissues. For each needle, 1700 images (2 s each) were recorded during the 360° rotation of the sample. Total scan

time was <1 h and final spatial resolution was 2.5 × 2.5 × 2.5 μm^3 per voxel. Full 3D volumes were reconstructed by datos|x 2.0 (Phoenix, Nanotom 180 XS, GE, Wunstorf, Germany) software and volumic image analysis and display, including 2D slice extraction, were performed using VGStudio Max© 2.1 software (Volume Graphics, Heidelberg, Germany).

After imaging, the needle was removed and its *P* value determined. The difference between *P* measured on needles before and after microtomography observations was always <0.2 MPa at maximum.

Statistics

All values are given as mean ± SE (the number of samples is included in tables or given in the text). Differences were tested with Student's *t*-test after testing for Gaussian distribution (Kolmogorov–Smirnov test) and variance homogeneity (Levene test) of data. In the case of inhomogeneous variances, Welch's test (difference in k_s between stems and needles) was used. All tests (two-tailed) were performed pairwise at a probability level of 5% using SPSS (Ver. 15.0, SPSS Inc., Chicago, IL, USA).

Results

Hydraulic conductivity and vulnerability to drought-induced embolism of needle xylem

Pressure at 50% loss of conductivity (P_{50}) in stem xylem was –3.6 MPa with the cavitron and slightly higher with the acoustic method (–3.2 MPa). P_{50} of needle xylem was less negative with only ~– 1.5 MPa measured with both methods (Table 1 and Figure 1). Vulnerability curves obtained from acoustic measurements were steeper than those from cavitron measurements, particularly for needles.

The hydraulic conductivity measured with the cavitron technique was 2.0×10^{-4} m^2 s^{-1} MPa^{-1} in needle xylem and 7.7×10^{-4} m^2 s^{-1} MPa^{-1} in stem xylem. We assume that cavitron measurements on needles, cut open at both ends, predominantly reflected flow capacities of the central xylem cylinder. We do not expect (Cochard et al. 2007) but cannot completely rule out effects of the low temperature on measurements (also see Materials and methods). Interestingly, flow rates in the cavitron took several minutes (10 to 20 min, Figure 1) to stabilize after each step down in water potential. This was probably related to emptying of mesophyll parenchyma, which buffered changes in water potential.

Table 1. Pressure at 50% loss of conductivity (P_{50}; MPa) in stems and needles of *P. pinaster* estimated with the centrifuge (water potential at 50% PLC) and ultrasonic (water potential at 50% cumulative number of UEs) method and conductivity (*ks*; m^2 s^{-1} MPa^{-1} 10^{-4}) of axe and needle xylem estimated with the centrifuge method. P_{50} values in each row not followed by the same letter differ significantly. Significant differences between stems and needles (within rows) are marked by asterisks. Mean ± SE. $P \leq 0.05$. *n* = number of samples.

	Centrifuge	Ultrasonic	k_s	*N*
Stems	–3.55 ± 0.13^a	–3.15 ± 0.09^b	7.74 ± 0.56	4/8/225
Needles	–1.43 ± 0.11^{a*}	–1.54 ± 0.06^{a*}	2.03 ± 0.08*	5/24/9

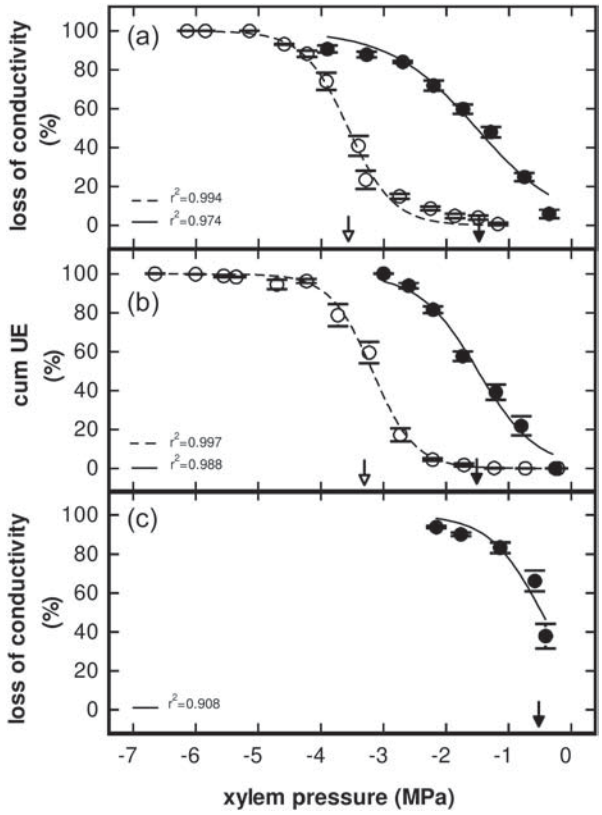

Figure 1. Vulnerability curves of needles (solid symbols) and stems (open symbols) of *P. pinaster*. Curves were fitted by the equation described in Pammenter and Vander Willigen (1998). Full and open arrows indicate needle and stems P_{50}. (a) Percentage loss of conductivity measured with centrifuge technique plotted against xylem pressure. (b) Percentage of cumulative number of UEs plotted against xylem pressure. (c) Percentage loss of conductivity of needles analysed with rehydration kinetics method plotted against xylem pressure.

Hydraulic conductance and vulnerability to drought-induced embolism of whole needles

The hydraulic conductance (K_{leaf}) of hydrated *P. pinaster* needles measured with the rehydration kinetics method was 6.7 mmol m^{-2} s^{-1} MPa^{-1}. Plotting K_{leaf} versus the water potential revealed a P_{50} for the whole needle of ca. –0.5 MPa. This method did not enable us to distinguish between effects of cell collapse and embolism formation in the xylem.

Visualization of wall deformation and cavitation in needle tissues at different *P*

The 3D pictures obtained by both the X-ray microtomography (Figure 3) system and cryo-SEM (Figure 2) revealed xylem

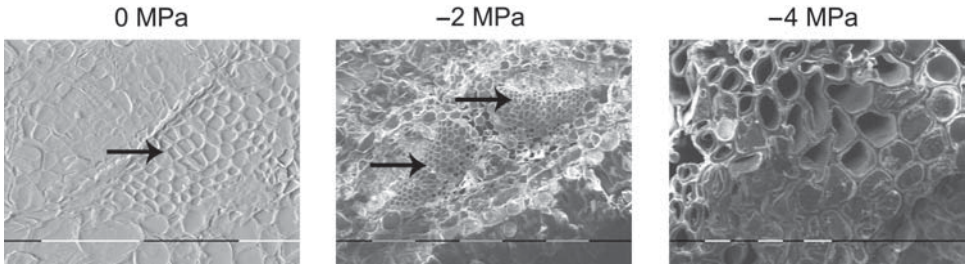

Figure 2. Cryo-SEM pictures of vascular bundles in *P. pinaster* needle cross sections at different xylem pressures. Arrows indicate the xylem. Scale bar represents 100 µm (0 and –2 MPa) and 10 µm (–4 MPa).

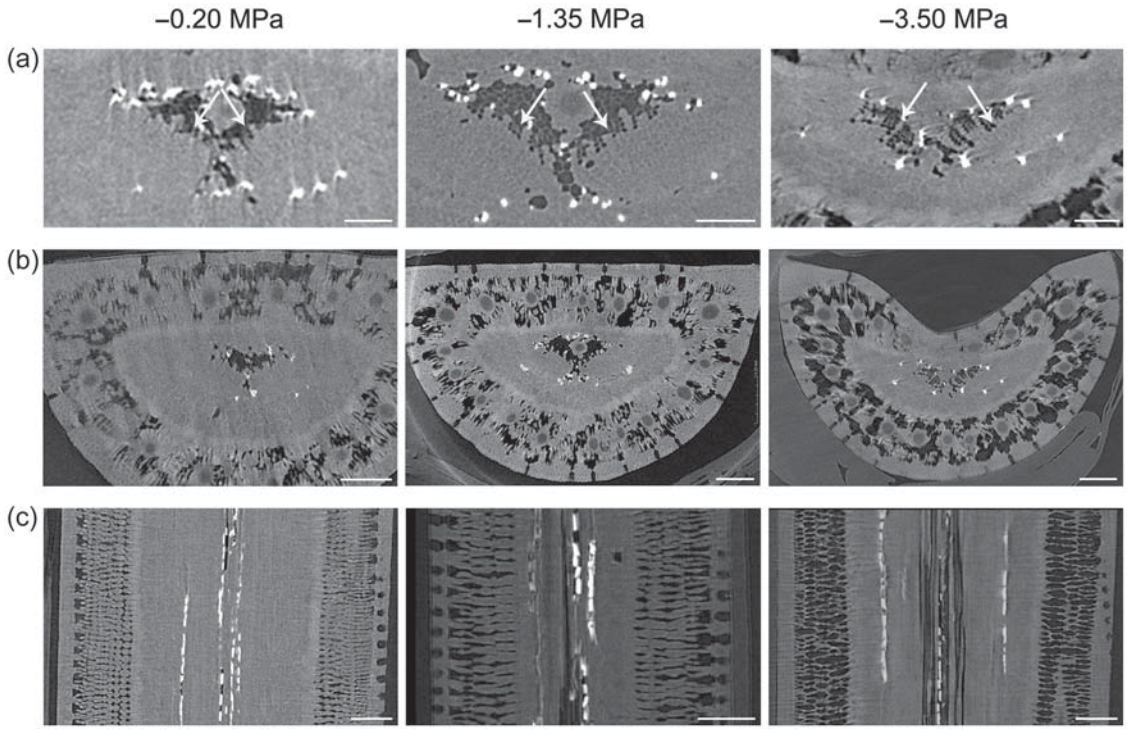

Figure 3. X-ray microtomography cross sections of vascular bundles (a) and whole needles (b) of *P. pinaster* at different xylem pressures. (c) Longitudinal sections. Scale bar represents 100 µm (a) and 200 µm (b and c).

cavitation events at –1.35 and –2.00 MPa, respectively. At more negative *P* (–3.5 and –4.0 MPa), cavitation occurred in a large part of the xylem, but some tracheids seemed still functional. With the microtomograph, the contrast between free water in lumens and cell wall was very low. Thus, using only transversal views, it was difficult to visualize xylem structures when they were fully saturated, and the extent of xylem embolism. However, using the full 3D information, cross and longitudinal slices were observed and it was possible to localize the xylem on sharp pictures, and even to discern tracheid walls. Collapse and cavitation events were first observed more often in 'old' tracheids on the external side of the xylem, as already observed by Cochard et al. (2004*a*), while small, flat 'young' tracheids alongside the phloem were either very resistant to dehydration or unaffected (Figure 2). Surprisingly, a part of the parenchyma cells between the two xylem cylinders seemed already air-filled at –0.2 MPa (Figure 3). Cryo-SEM pictures of needles dehydrated at –2 and –4 MPa revealed cell collapse and cavitation in tracheids, in the xylem parenchyma cells and in the transfusion tissue. Collapsed cells were also detected with microtomography: we observed that the endodermis became compressed and air-filled space appeared in the mesophyll tissue (gaps).

Discussion

Conifer needle hydraulics have, up to now, been much more difficult to analyse methodically than angiosperm leaves. Needles are much smaller, often contain resin ducts and exhibit low hydraulic conductivities. In the present study, the use of

several new methods such as the cavitron technique and X-ray microtomography provided new insights into hydraulic efficiency and safety of pine needles. However, hydraulic and acoustic measurements on conifer needles need some caution, since they are still not as reliable as on broad leaves, and they do not fit exactly with visualization.

Hydraulic efficiency and safety of needle xylem

The xylem of *P. pinaster* needles showed a k_s value of 2.03×10^{-4} m^2 s^{-1} MPa^{-1}, consistent with Charra-Vaskou and Mayr (2011), who determined a k_s of 3.5×10^{-4} m^2 s^{-1} MPa^{-1} and 0.9×10^{-4} m^2 s^{-1} MPa^{-1} in *P. abies* and *P. mugo*. Furthermore, stem xylem conductivity (7.7×10^{-4} m^2 s^{-1} MPa^{-1}) was slightly higher than needle xylem conductivity, as in Charra-Vaskou and Mayr (2011).

It is known that a major portion of the resistance is located at the pits. Pittermann et al. (2006) reported that 64 ± 4% of total hydraulic resistance was related to end wall pitting across 19 conifer species. We calculated the theoretical conductivity of the xylem in *P. pinaster* needles by analysis of tracheid diameters in needle cross sections and estimating the tracheid conductance according to the Hagen–Poiseuilles equation. We found k_s values measured using the cavitron to be only 9.5% of this theoretical conductivity (21.4×10^{-4} m^2 s^{-1} MPa^{-1}). As a pit resistance of >90% is unlikely, this may indicate that some tracheids were dysfunctional even in non-drought-stressed needles.

The transfusion tissue, located between vascular cylinder and endodermis, and the mesophyll tissue, made up of layers of palisade cells containing chloroplasts and located between endodermis and hypodermis, are thought to be responsible for radial water transport (Zwieniecki et al. 2004, Sack and Holbrook 2006, Zwieniecki et al. 2006). The role of the apoplastic or symplastic/transcellular radial pathway is not yet known (Sack and Holbrook 2006). A relevant contribution to axial transport is unlikely, as indicated by Charra-Vaskou and Mayr (2011) and by staining experiments (K. Charra-Vaskou and S. Mayr, unpublished data).

Like angiosperm leaf veins (Salleo et al. 2000, Choat et al. 2005, Hao et al. 2008, Chen et al. 2009), needle xylem was more vulnerable to drought-induced loss of conductivity than stem xylem. While collapse has never been observed in conifer stems, some studies have reported collapse and (or) cavitation in conifer needles (Cochard et al. 2004*a*, Brodribb and Holbrook 2005). Needle tracheid collapse could be due to lower conduit wall thickness to span ratio (Hacke et al. 2001, 2004), differences in chemical composition of the cell wall (Turner and Somerville 1997) and (or) differences in bordered pits (Hacke et al. 2004). Cochard et al. (2004*a*) reported a correlation between the onset of wall collapse in needles and cavitation in twigs of *Pinus* species: *P. nigra* was thus the most vulnerable species (needle collapse pressure –1.8 MPa) and *Pinus cembra* L. the least (needle collapse pressure –3.5 MPa).

For *P. pinaster*, pressure to induce 50% loss of conductivity (P_{50}) in needle xylem was only –1.43 ± 0.11 MPa, while P_{50} of stem xylem was –3.55 ± 0.13 MPa based on the cavitron measurements (Table 1; Figure 1a). In this study, we could not precisely distinguish between collapse and cavitation effects in needles. According to the concept of vulnerability segmentation (Tyree and Zimmermann 2002, Mayr et al. 2003), distal plant parts are often more vulnerable, while proximal parts are protected from embolism.

Ultrasonic emission analysis revealed similar vulnerability thresholds (Table 1, Figure 1). Ultrasonic emission analyses are normally used with massive xylem samples, while measurements on needles were expected to be more difficult. First, all water-filled cells may cause UEs on cavitation so that non-conductive cells will influence the UE-based VC, but have no effect on hydraulic conductivity. Second, it is not known as to whether each ultrasonic event is related to exactly one cavitation event. It is likely that conduits cavitate in groups, so that the UE numbers do not exactly reflect the number of dysfunctional conduits. Third, the number of UEs does not distinguish between conduits of different sizes, which has large hydraulic effects (Tyree and Dixon 1983, Tyree et al. 1984, Mayr and Rosner 2011). Finally, it is unknown as to whether collapse events, which are of relevance in conifer needles (Cochard et al. 2004*a*), may also cause UEs. However, despite these uncertainties, UEs seem to sufficiently reflect vulnerability thresholds. Johnson et al. (2009), who also used the UE method, observed a P_{50} of –1.39 and –1.94 MPa in needles of *P. nigra* and *P. ponderosa*, respectively.

Hydraulic efficiency and safety patterns within needles

Pinus pinaster whole needles showed a K_{leaf} value of 6.71 mmol m^{-2} s^{-1} MPa^{-1}, in line with findings of other authors: Sack and Holbrook (2006) reported a conifer K_{leaf} around 6.6 mmol m^{-2} s^{-1} MPa^{-1}, Brodribb and Holbrook (2005) found a K_{leaf} of 6.7 mmol m^{-2} s^{-1} MPa^{-1} in *Podocarpus grayae* de Laub., Woodruff et al. (2007) 3–5.5 mmol m^{-2} s^{-1} MPa^{-1} in *Pseudotsuga menziesii* (Mirb.) Franco and Charra-Vaskou and Mayr (2011) 1.8 mmol m^{-2} s^{-1} MPa^{-1} in *P. mugo*.

Based on conductance measurements via rehydration kinetics, P_{50} of the whole needle was –0.47 ± 0.10 MPa (Table 1). In *P. nigra* and *P. ponderosa* needles, P_{50} was –1.52 and –1.65 MPa, respectively (Johnson et al. 2009), and –0.91 MPa in *P. taeda* (Domec et al. 2009). P_{50} of the whole *P. pinaster* needles was ~1 MPa less negative than P_{50} of the needle xylem (Table 1, Figure 1), which indicates that the hydraulic extra-vascular pathway is more vulnerable than the vascular section within needles. We cannot totally rule out the possibility that a part of this difference in P_{50} is related to resin effects, although several test measurements were performed (see Materials and methods). Johnson et al. (2012) also reported that the hydraulic pathway outside the leaf xylem plays a key

role for vulnerability thresholds of needles. In *P. ponderosa,* Johnson et al. (2009) found 50% loss of K_{leaf} at ~0.3 MPa less negative pressure than 50% of cumulative UEs, while P_{50} with the two methods was similar in *P. nigra.* Brodribb and Holbrook (2005) reported that collapse of lignified peripheral tracheids in *Podocarpus grayae* de Laub. leaves was closely correlated to a decline in K_{leaf}, and occurred before cavitation-induced loss of hydraulic conductance in leaf veins. This high vulnerability to drought of the whole needle may be offset by the large capacitance typically displayed by conifer leaves (Brodribb and Holbrook 2005, Brodribb et al. 2005, Johnson et al. 2009). Johnson et al. (2011) also suggested that it might be comparably easy to refill small conifer needles.

Visualization of needle tissues during dehydration

Cochard et al. (2004*a*) reported a Cryo-SEM study indicating xylem wall collapse in the needles of four conifer species at water potentials above cavitation thresholds. In contrast, Woodruff et al. (2007) showed that tracheids in Douglas fir needles were liable to embolize even under non-extreme environmental conditions without previous collapse, and Brodribb and Holbrook (2005) showed that tracheids in the midvein of *P. grayae* leaves were not prone to collapse. Cryo-SEM images also confirmed that cavitation occurred in *P. ponderosa* needles (Johnson et al. 2009). Surfactant experiments also indicated that embolism was responsible for K_{leaf} decline in four angiosperms and one coniferous species (*P. ponderosa*; Johnson et al. 2012). Needles of *P. pinaster* showed both cavitated and collapsed tracheids in needles dehydrated to −4.0 or −3.5 MPa (Figure 2).

Strikingly, collapsed or embolized xylem portions observed with the Cryo-SEM did not correspond closely to VCs established with the hydraulic or the UE method. Vulnerability curves predicted a PLC of >90% at a water potential of −3.5 or −4 MPa, while only 20–70% of tracheids showed collapse or embolism in Cryo-SEM and X-ray microtomography pictures (Figures 2 and 3). Like theoretical k_s calculations (see Results), this may also indicate that some parts of the needle xylem do not contribute to longitudinal water transport. These tracheids may have a mechanical function. However, while artefacts seemed to be ruled out of visualization methods, hydraulic and acoustic measurements need greater caution. The discrepancy between the two measurement methods emphasizes that hydraulic and acoustic methods need further study to become reliable for needles of different species.

Three-dimensional microtomographic observations (Figure 3) revealed striking changes in xylem parenchyma cells during dehydration. These elongated cells were located within and around the xylem bundle. Even at moderate dehydration, large gaps were visible in this parenchyma tissue. The same was observed by Johnson et al. (2009), who reported that most transfusion tissue surrounding the vascular bundles in *P. ponderosa* was empty at a *P* corresponding to 4% of accumulated UEs and ~92% of maximum K_{leaf}. Living cells adjacent to xylem conduits may be important for refilling mechanisms (Johnson et al. 2012) and could be involved in radial water transport (Holbrook and Zwieniecki 1999). The gaps in parenchyma tissue may explain the early loss of conductivity observed in whole needles (Johnson et al. 2011). When parenchyma cells surrounding the xylem are hydraulically dysfunctional, radial water transport may be affected, leading to a modification in needle vein permeability and a pressure drop in the xylem (Zwieniecki et al. 2006). Also, Brodribb and Holbrook (2005) found the radial pathway to be more vulnerable than the xylem in conifer leaves. We also found indications for collapse within the transfusion tissue, which also plays an important role in radial transport (Figure 3).

On X-ray microtomography pictures, many high-density structures around the bundle were observed, represented as white cylinders, which could not be identified. The mesophyll, which contributes ~68% of the needle cross-section area, also showed increasing gaps in dehydrating needles. Unfortunately, it was not possible to distinguish intracellular openings from extracellular gaps. As indicated by variations in mesophyll area during dehydration (Figure 3), it may be hydraulically important as a buffer to withstand short-term fluctuations in water potential. Future studies should focus especially on the reversibility of observed structural changes. We suggest that these changes are reversible to fulfil a buffer function and thereby protect the xylem from embolism.

X-ray microtomography gave new insights into the local water status in the anatomical structure of needles tissues and their modifications during exposure to drought stress. This relatively new method enabled us to view a whole needle in three dimensions many times during dehydration with no cutting or treatment, which should reduce preparation artefacts. However, up to now it has not been possible to explain all the effects, and especially the discrepancy between measurement and visualization of cavitation events. The methodological problems that could cause artefacts cannot all be totally excluded, although such an explanation seems unlikely for visualization methods. Further experiments will be required to link observed structural changes and functional aspects.

Conclusion

Pinus pinaster, like many other trees, seems to show higher vulnerabilities at the most distal parts of the soil–plant–atmosphere continuum. This vulnerability pattern is one aspect of this species' hydraulic architecture with further hydraulic complexity at the level of needles. Our results indicate that the most distal, radial hydraulic pathway in the needle exhibits a low hydraulic efficiency and low hydraulic safety. Living tissues around the xylem thus may substantially limit needle

transport capacities, but may also be involved in buffering short-term water deficits, thus averting xylem embolism. Further investigation on different species is now required to gain a fuller understanding of the discrepancy between hydraulic measurements and the visualizations we propose as references tools.

Acknowledgments

The authors thank Jean-Baptiste Lamy for help with cavitron measurements and Thierry Améglio for organizing stays in Clermont-Ferrand.

Conflict of interest

None declared.

Funding

This study was supported by the Austrian Science Fund (FWF), P18514-B03 and P20852-B16 and the University of Innsbruck (Auslandsstipendium).

References

Beikircher B, Améglio T, Cochard H, Mayr S (2010) Limitation of the cavitron technique by conifer pit aspiration. J Exp Bot 61:3385–3393.

Blackman CJ, Brodribb TJ (2011) Two measures of leaf capacitance: insights into the water transport pathway and hydraulic conductance in leaves. Funct Plant Biol 38:118–126.

Brodribb TJ, Cochard H (2009) Hydraulic failure defines the recovery and point of death in water-stressed conifers. Plant Physiol 149:575–584.

Brodribb TJ, Holbrook NM (2003) Stomatal closure during leaf dehydration, correlation with other leaf physiological traits. Plant Physiol 132:2166–2173.

Brodribb TJ, Holbrook NM (2004) Diurnal depression of leaf hydraulic conductance in a tropical tree species. Plant Cell Environ 27:820–827.

Brodribb TJ, Holbrook NM (2005) Water stress deforms tracheids peripheral to the leaf vein of a tropical conifer. Plant Physiol 137:1139–1146.

Brodribb TJ, Holbrook NM, Zwieniecki MA, Palma B (2005) Leaf hydraulic capacity in ferns, conifers and angiosperms: impacts on photosynthetic maxima. New Phytol 165:839–846.

Brodribb TJ, Field TS, Jordan GJ (2007) Leaf maximum photosynthetic rate and venation are linked by hydraulics. Plant Physiol 144:1890–1898.

Charra-Vaskou K, Mayr S (2011) The hydraulic conductivity of the xylem in conifer needles (*Picea abies* and *Pinus mugo*). J Exp Bot 6:4383–4390.

Chen JW, Zhang Q, Li XS, Cao KF (2009) Independence of stem and leaf hydraulic traits in six Euphorbiaceae tree species with contrasting leaf phenology. Planta 230:459–468.

Choat B, Lahr EC, Melcher PJ, Zwieniecki MA, Holbrook M (2005) The spatial pattern of air seeding thresholds in mature sugar maple trees. Plant Cell Environ 28:1082–1089.

Cochard H, Tyree MT (1990) Xylem dysfunction in *Quercus*: vessel sizes, tyloses, cavitation and seasonal changes in embolism. Tree Physiol 6:393–407.

Cochard H, Bodet C, Améglio T, Cruiziat P (2000*a*) Cryo-scanning electron microscopy observations of vessel content during transpiration in walnut petioles. Facts or artefacts? Plant Physiol 124:1191–1202.

Cochard H, Martin R, Gross P, Bogeat-Triboulot MB (2000*b*) Temperature effects on hydraulic conductance and water relations of *Quercus robur* L. J Exp Bot 51:1255–1259.

Cochard H, Froux F, Mayr S, Coutand C (2004*a*) Xylem wall collapse in water-stressed pine needles. Plant Physiol 134:401–408.

Cochard H, Nardini A, Coll L (2004*b*) Hydraulic architecture of leaf blades: where is the main resistance? Plant Cell Environ 27:1257–1267.

Cochard H, Damour G, Bodet C, Tharwat I, Poirier M, Améglio T (2005) Evaluation of a new centrifuge technique for rapid generation of xylem vulnerability curves. Physiol Plant 124:410–418.

Cochard H, Barigah T, Herbert E, Caupin F (2007) Cavitation in plants at low temperature: is sap transport limited by the tensile strength of water as expected from Briggs' Z-tube experiment? New Phytol 173:571–575.

Cochard H, Hölltä T, Herbette S, Delzon S, Mencuccini M (2009) New insights into the mechanisms of water-stress-induced cavitation in conifers. Plant Physiol 151:949–954.

Delzon S, Douthe C, Sala A, Cochard H (2010) Mechanism of water-stress-induced cavitation in conifers: bordered pit structure and function support the hypothesis of seal capillary-seeding. Plant Cell Environ 33:2101–2111.

Domec JC, Palmroth S, Ward E, Maier CA, Thérézien M, Oren R (2009) Acclimation of leaf hydraulic conductance and stomatal conductance of *Pinus taeda* (loblolly pine) to long-term growth in elevated CO_2 (free-air CO_2 enrichment) and N-fertilization. Plant Cell Environ 32:1500–1512.

Gasco A, Nardini A, Salleo S (2004) Resistance to water flow through leaves of *Coffea arabica* is dominated by extra-vascular tissues. Funct Plant Biol 31:1161–1168.

Hacke UG, Sperry JS, Pockman WT, Davis SD, McCulloh A (2001) Trends in wood density and structure are linked to prevention of xylem implosion by negative pressure. Oecologia 126:457–461.

Hacke UG, Sperry JS, Pittermann J (2004) Analysis of circular bordered pit function II. Gymnosperm tracheids with torus-margo pit membranes. Am J Bot 91:386–400.

Hao GY, Hoffmann WA, Scholz FG, Bucci SJ, Meinzer FC, Franco AC, Cao KF, Goldstein G (2008) Stem and leaf hydraulics of congeneric tree species from adjacent tropical savanna and forest ecosystems. Oecologia 155:405–415.

Holbrook NM, Zwieniecki MA (1999) Embolism repair and xylem tension: do we need a miracle? Plant Physiol 120:7–10.

Hukin D, Cochard H, Dreyer E, Le Thiec D, Bogeat-Triboulot MB (2005) Cavitation vulnerability in roots and shoots: does *Populus euphratica* Oliv., a poplar from arid areas of Central Asia, differ from other poplar species? J Exp Bot 56:2003–2010.

Johnson DM, Meinzer FC, Woodruff DR, McCulloh KA (2009) Leaf xylem embolism, detected acoustically and by cryo-SEM, corresponding to decrease in leaf hydraulic conductance in four evergreen species. Plant Cell Environ 32:828–836.

Johnson DM, McCulloh KA, Meinzer FC, Woodruff DR (2011) Hydraulic patterns and safety margins, from stem to stomata, in three eastern US tree species. Tree Physiol 31:659–668.

Johnson DM, McCulloh KA, Woodruff DR, Meinzer FC (2012) Evidence for xylem embolism as a primary factor in dehydration-induced declines in leaf hydraulic conductance. Plant Cell Environ 35:760–769.

Mayr S, Cochard H (2003) A new method for vulnerability analysis of small xylem areas reveals that compression wood of Norway spruce has lower hydraulic safety than opposite wood. Plant Cell Environ 26:1365–1371.

Mayr S, Rosner S (2011) Cavitation in dehydrating xylem of *Picea abies*: energy properties of ultrasonic emissions reflect tracheid dimensions. Tree Physiol 31:59–67.

Mayr S, Sperry J (2010) Freeze-thaw-induced embolism in *Pinus contorta*: centrifuge experiments validate the 'thaw-expansion hypothesis' but conflict with ultrasonic emission data. New Phytol 185:1016–1024.

Mayr S, Rothart B, Dämon B (2003) Hydraulic efficiency and safety of leader shoots and twigs in Norway spruce growing at the alpine timberline. J Exp Bot 54:2563–2568.

Nardini A, Salleo S (2000) Limitation of stomatal conductance by hydraulic traits: sensing or preventing xylem cavitation? Trees Struct Funct 15:14–24.

Nardini A, Salleo S, Andri S (2005) Circadian regulation of leaf hydraulic conductance in sunflower (*Helianthus annuus* L. cv Margot). Plant Cell Environ 28:750–759.

Pammenter NW, Vanderwilligen C (1998) A mathematical and statistical analysis of the curves illustrating vulnerability of xylem to cavitation. Tree Physiol 18:589–593.

Pittermann J, Sperry JS, Hacke UG, Wheeler JK, Sikkema EH (2006) Inter-tracheid pitting and the hydraulic efficiency of conifer wood: the role of tracheid allometry and cavitation protection. Am J Bot 93:1265–1273.

Sack L, Holbrook M (2006) Leaf hydraulics. Annu Rev Plant Biol 57:361–381.

Sack L, Cowan PD, Jaikumar N, Holbrook NM (2003) The 'hydrology' of leaves: coordination of structure and function in temperate woody species. Plant Cell Environ 26:1343–1356.

Sack L, Streeter CM, Holbrook NM (2004) Hydraulic analysis of water flow through leaves of sugar maple and red oak. Plant Physiol 134:1824–1833.

Sack L, Tyree MT, Holbrook NM (2005) Leaf hydraulic architecture correlates with regeneration irradiance in tropical rainforest trees. New Phytol 167:403–413.

Salleo S, Nardini A, Pitt F, Lo Gullo MA (2000) Xylem cavitation and hydraulic control of stomatal conductance in laurel (*Laurus nobilis* L.). Plant Cell Environ 23:71–79.

Sperry JS, Tyree MT (1988) Mechanism of water stress-induced xylem embolism. Plant Physiol 88:581–587.

Sperry JS, Tyree MT (1990) Water-stress-induced xylem embolism in three species of conifers. Plant Cell Environ 13:427–436.

Trifilo P, Nardini A, LoGullo MA, Salleo S (2003) Vein cavitation and stomatal behaviour of sunflower (*Helianthus annuus*) leaves under water limitation. Physiol Plant 119:409–417.

Turner SR, Somerville CR (1997) Collapsed xylem phenotype of *Arabidopsis* identifies mutants deficient in cellulose deposition in the secondary cell wall. Plant Cell 9:689–701.

Tyree MT, Dixon MA (1983) Cavitation events in *Thuja occidentalis* L.? Ultrasonic acoustic emissions from the sapwood can be measured. Plant Physiol 72:1094–1099.

Tyree MT, Sperry JS (1988) Do woody plants operate near the point of catastrophic xylem dysfunction caused by dynamic water stress? Answer from a model. Plant Physiol 88:0574–0580.

Tyree MT, Zimmermann MH (2002) Xylem structure and the ascent of sap. Springer, Berlin.

Tyree MT, Cruiziat P, Benis M, LoGullo MA, Salleo S (1981) The kinetics of rehydration of detached sunflower leaves from different initial water deficits. Plant Cell Environ 4:309–317.

Tyree MT, Dixon MA, Tyree EL, Johnson R (1984) Ultrasonic acoustic emissions from the sapwood of cedar and hemlock. An examination of three hypotheses regarding cavitations. Plant Physiol 75:988–992.

Tyree MT, Davis SD, Cochard H (1994) Biophysical perspectives of xylem evolution: is there a tradeoff of hydraulic efficiency for vulnerability to dysfunction? IAWA J 15:335–360.

Woodruff DR, McCulloh KA, Warren JM, Meinzer FC, Lachenbruch B (2007) Impacts of tree height on leaf hydraulic architecture and stomatal control in Douglas-fir. New Phytol 180:90–99.

Yang SD, Tyree MT (1994) Hydraulic architecture of *Acer saccharum* and *A. rubrum*: comparison of branches to whole trees and the contribution of leaves to hydraulic resistance. J Exp Bot 45:179–186.

Zwieniecki MA, Boyce CK, Holbrook NM (2004) Functional design space of single-veined leaves: role of tissue hydraulic properties in constraining leaf size and shape. Ann Bot 94:507–513.

Zwieniecki MA, Stone HA, Leigh A, Boyce CK, Holbrook NM (2006) Hydraulic design of pine needles: one-dimensional optimization for single-vein leaves. Plant Cell Environ 29:803–809.